Journal of the Iranian Chemical Society
https://doi.org/10.1007/s13738-020-01983-2

ORIGINAL PAPER

Rare earth Ce- and Nd-doped spinel nickel ferrites as effective heterogeneous catalysts in the (ep)oxidation of alkenes

Mohamed Shaker S. Adam[1,2] · **Aly M. Hafez**[1] · **Mai M. Khalaf**[1,2]

Received: 3 April 2020 / Accepted: 16 June 2020
© Iranian Chemical Society 2020

Abstract

Cerium (Ce)- and neodymium (Nd)-doped spinel nickel ferrites catalysts system were synthesized using a cost-effective sol–gel route. The as-prepared nickel ferrites and its doped Ce and Nd nanomaterials were characterized in terms of Fourier transform infrared spectrophotometry, X-ray diffraction, field emission scanning electron microscopy, energy-dispersive X-ray spectroscopy, transmission electron microscopy, selected area diffraction pattern, zeta potential and magnetism techniques. Their catalytic potential was examined in the (ep)oxidation of 1,2-cyclooctene by using hydrogen peroxide (H_2O_2) or *tert*-butylhydroperoxide (*t*-BuOOH). Optimization of various parameters, including solvent, oxidant and catalyst type revealed that chloroform ($CHCl_3$) or 1,2-dichloroethane as a solvent and *t*-BuOOH as an oxidant were found to be the best choice for this catalytic system. The catalytic efficiency was found as Nd–$NiFe_2O_4$ > Ce–$NiFe_2O_4$ > $NiFe_2O_4$. Further, the applied nanocatalysts could be easily renovated and exhibited high catalytic reactivity for 5 times of recycling experiments with long-time durability. A reasonable discussion of the mechanism reaction reinforced the action of these spinel catalysts.

Keywords Nickel ferrite · Cerium- and neodymium-doped · Nanoparticles · Catalysis · (Ep)oxidation

Introduction

A massive achievement in nanotechnology and nanoscience fields induces the searching for advanced synthetic procedures of various mixed metal oxides, as nanomaterials, with crucial physicochemical characteristics in alternative applicable proposes [1]. Among those uncountable mixed metal oxides [2], the magnetic spinel nanostructured ferrites, MFe_2O_4 ($M = Co^{2+}$, Mn^{2+}, Ni^{2+} and Cu^{2+}), have gained great regards of high chemical stability and marvelous magnetic features [3, 4]. This meets the requirements for wide applications, e.g., solar energy transformation [5, 6], gas sensors [7], magnetic storage materials [8, 9], catalytic reagents [10–13], ferrofluids [14] and drug delivery systems [15]. Moreover, spiral ferrites are used in medical proposes, e.g., drug delivery, bio-molecules, bio-sensors and magnetic separation of cells [16, 17].

The soft ferrites with interesting structural features have an appropriate dielectric loss and low cost. The main advantage of the spinel ferrites is the reduction of the particle size in the nanoscales with observable magnetic losses and new electromagnetic characteristics [18]. Spinel ferrites show appreciable crystallinity of cubic structure, fine texture and structure control [9]. The structural and chemical features of spinel ferrites are extremely influenced by the synthetic pathway and their chemical compositions, which could promote their applicability. The spinel ferrites could be classified into three categories. The first type is the normal spinel, the second type is the inverse spinel, and the third type is the intermediate spinel. Moreover, there are other two additional categories; the inverse spinel, which are the most attractive in research, resulted from their progressed saturated magnetization [19]. In particular, nickel ferrite has an inverse spinel structure, whereas the doped spinel ferrites with additional cations provide various physical properties depending upon their composition [20].

Electronic supplementary material The online version of this article (https://doi.org/10.1007/s13738-020-01983-2) contains supplementary material, which is available to authorized users.

✉ Mohamed Shaker S. Adam
madam@kfu.edu.sa; shakeradam61@yahoo.com

[1] Department of Chemistry, College of Science, King Faisal University, P.O. Box 380, Al Hofuf 31982, Al-Ahsa, Saudi Arabia

[2] Chemistry Department, Faculty of Science, Sohag University, Sohag 82534, Egypt

Published online: 05 July 2020

As of great attention, magnetic spinel nanostructured materials are considered as metal-based catalysts in the view of their high dispersion, low oxidation potentials, ecological protection, less toxicity, higher stability and proper catalyst reprocessing. Accordingly, spinel ferrites and their reported doped nanospecies were involved as sufficient catalysts for many industrial applicable oxidative proposes [21]. The oxidation of glucose a graphite paste electrode was accomplished by $NiFe_2O_4$ nanoparticles, which was reported by Galindo et al. [22]. Furthermore, the catalytic properties of nickel ferrites were examined recently in the oxidation of glucose, β-nicotiamide adenine dinucleotide and methanol by the same previous working group [23]. The chemoselective oxidation of thiols to disulfides and sulfides to sulfoxides using H_2O_2 and catalyzed by $NiFe_2O_4$-nanoparticles was studied by Kulkarni et al. [24] with the suggestion of a mechanistic pathway. The Aerobic oxidation of benzyl alcohol by air oxygen and catalyzed by $NiFe_2O_4$-nanoparticles was reported recently [25]. The catalytic oxidation of aqueous sulfide to polysulfides was studied by Cunha et al. [26] in the presence of various metal ferrites (MFe_2O_4, $M = Fe^{2+}$, Cu^{2+} and Co^{2+}), as heterogeneous catalysts. Nickel ferrite nanoparticles were applied as highly durable catalysts for catalytic transfer hydrogenation of bio-based aldehydes [27]. The retrievable modified nickel ferrite nanoparticles were used as efficient catalysts for the reduction of nitroarenes and for the photo-oxidation of hazardous Dyes, which were reported by Goyal et al. [28]. For the metal-doped spinel nickel ferrites, some rare earth elements (La, Sm, Gd and Dy)-doped spinel nickel ferrites were used as heterogeneous catalysts for the wet hydrogen peroxide oxidation of Orange II azo-dye [29]. Moreover, the ethyl acetate oxidation was investigated catalytically by copper-doped nickel ferrites catalyst [30].

As a consequence, numerous date approaches like mechanical milling [31], sol–gel [32], hydrothermal [33], micro-emulsion [34], reverse micelle [35], co-precipitation [36], polymer matrix-mediated synthesis and ultrasonic-assisted hydrothermal processes [37] are widely proposed to attain distinct nanostructured spinel ferrites.

The sol–gel method is considered as one of the most promising eco-friendly methods, which utilized to prepare alternative mixed metal oxides, nanomaterials and nanoporous mixed metal oxides [38–41]. This method has abundant advantages including forming of mixed sol of the precursors and good homogeneous desired solid products. Additionally, the sol–gel process is considered a cost-effective and easy preparation procedure for the formation of nanoparticles. It is noteworthy that the porous texture of the resulting nanomaterials could be obtained by the hydrolysis of the reacted species, forming prolonged networks with reducing of the synthetic temperature. In the sol–gel method, the employed organic acids or polymers, as structure-directing templates, which are bounded to the metal ion, could be easily rearranged resulting in the cubic spinel ferrites structure [40, 41]. Hence, the spinel structure of the metal-fed nickel ferrites could be employed as heterogeneous catalysts for selective catalytic oxidation processes due to the entrapment of the reactant species on its surface [42]. Moreover, the rare earth doping ferrites could strongly be imperative for the high-performance catalytic processes, which was attributed to oxygen vacancies effect and the alteration of metal valences.

The design of benefit catalysts (homogeneously or heterogeneously) in the control olefins (ep)oxidation has a curial impact in the industrialized protocols of the dreamt organic syntheses, economically and sustainably through the diminution of the formation of unwelcomed harmful wastes attracted many researchers' interest [42–44]. Transition metal-chelating complexes were widely reported as the most valuable catalysts for the alkenes (ep)oxidation to the corresponding chemoselective epoxides, which were operated by various oxidizing agents, attractively, molecular oxygen and hydrogen peroxide (H_2O_2), as the most eco-friendly oxidants. The most effective metal-based catalysts, which be utilized for the alkene (ep)oxidation, should gain features with high Lewis acidity and high oxidation states, e.g., molybdenyl and vanadyl species in the homogeneous phase [43]. Although the homogeneous metal-chelates exhibit higher activity per unit mass of metal than the heterogeneous catalysts, e.g., metal oxides [45], the heterogeneous catalysts have additional advantages over the homogeneous ones, as automatically removed and recovered from the process and the plentiful reusability [42]. In another word, reusability and extraction of the catalysts were the main difficulties in such homogeneous processes. Hence, recent researches have shed light on the use of new heterogeneous catalysts in the (ep)oxidation processes with recycling character and easy extraction. Various types of heterogeneous catalysts could be designed to be easily separated and recycled [46]. An early study was investigated using nickel spinel ferrites with high magnetic features for the selective (ep)oxidation of 1,2-cyclooctene in the existence of *tert*-butyl hydroperoxide (*t*-BuOOH), as an oxidant, in CCl_4. The recyclability of such catalysts was up to 4 times, losing only 13% of its potentials, which was qualified in chemical industry applications [46]. The strong demand of the Lewis acid character [47] of the applicable catalyst in the oxidation protocols reinforced to use the spinal ferrites doped by rare earth elements could remarkably enhance their catalytic behavior and reusability [48].

However, few previous works, which studied the (ep)oxidation of alkenes catalyzed by such soft ferromagnetic spinel ferrites, were reported [46, 48]. In this work, we investigate the morphology and crystallinity of the introduced $NiFe_2O_4$, Ce–$NiFe_2O_4$ and Nd–$NiFe_2O_4$ nanoparticles via FTIR, FE-SEM, TEM, XRD, EDS, zeta potential and magnetism (VSM) techniques. The catalytic efficiency of $NiFe_2O_4$ and its doped rare elements (Ce and Nd) as novel materials and heterogeneous catalysts in the alkene (ep)oxidation processes using aqueous H_2O_2 or *t*-BuOOH at different experimental conditions.

Experimental

Materials

The materials were of analytical grade and used as obtained. Iron nitrate nonahydrate Fe $(NO_3)_3{\cdot}9H_2O$ (99.99%), nickel nitrate hexahydrate $Ni(NO_3)_2{\cdot}6H_2O$ (97.0%), cerium nitrate hexahydrate $Ce(NO_3)_3{\cdot}6H_2O$ (99.999%), neodymium nitrate hexahydrate $Nd(NO_3)_3{\cdot}6H_2O$ (99.99%), 1,2-cyclooctene $(C_{10}H_{18})$ (95%), meso-tartaric acid monohydrate ≥ 97%, PEG $(H(OCH_2CH_2)_nOH)$, average molecular weight (M.wt) = 6500–7000 g/mol and all used solvents were received from Sigma-Aldrich, Merck and Acros. The materials were used as obtained without further purifications.

Preparation of $NiFe_2O_4$, Ce–$NiFe_2O_4$ and Nd–$NiFe_2O_4$

$NiFe_2O_4$ was prepared by dissolving the stoichiometric amounts of iron nitrate (0.01 M) and nickel nitrate hexahydrate (0.01 M) in 30 mL deionized water with magnetic stirring at room temperature. Then, 2.7 g of tartaric acid was added to the reaction mixture with continuous stirring for 30 min at room temperature. A specified amount of PEG (polyethylene glycol, 2.0 g) was added, as the structure-directing template, with further stirring for 15 min at room temperature. The obtained mixed sol was heated at 70 °C for 2 h. The viscous gel was centrifuged with extraction and then washed several times with ethanol and deionized water to remove undesired contaminants. The resulted sample was dried overnight at 100 °C in an oven and then ground to a fine powder. The acquired sample was calcined at 450 °C for 2 h with a rate of heating 10 °C min^{-1}. The final sample was coded as $NiFe_2O_4$.

For doped Ce–$NiFe_2O_4$ and Nd–$NiFe_2O_4$ preparation, the same method was used as mentioned for $NiFe_2O_4$ preparation with a further addition of $Ce(NO_3)_3{\cdot}6H_2O$ and $Nd(NO_3)_3{\cdot}6H_2O$ according to the composition of $Ce_xNi_{1-x}Fe_2O_4$ and $Nd_xNi_{1-x}Fe_2O_4$ ($x = 0.05$), and the obtained were coded as Ce–$NiFe_2O_4$ and Nd–$NiFe_2O_4$, respectively.

Characterization of $NiFe_2O_4$, Ce–$NiFe_2O_4$ and Nd–$NiFe_2O_4$

Characterization of the chemical morphology and structural features of the as-prepared pure $NiFe_2O_4$ and its doped Ce- and Nd-materials was examined using a Cary 630 FTIR spectrophotometer, which recorded within a frequency range from 400 to 4000 cm^{-1}. The XRD patterns were conducted with the help of a Burker D8 X-ray diffractometer with Ni-filtered Cu-Kα radiation and a graphite monochromator to produce X-rays with a wavelength of 1.54060 Å at 35 kV and 25 mA in a range of glancing—the angle from 10° to 80° at scan steps of 0.02° with an accuracy ≤ 0.001°. The surface morphology study was also conducted by transmission electron microscopy (TEM) (model: Jeol TEM-1230) operating at an acceleration voltage 120 kV and 20,000 magnifications and field emission scanning electron microscopy (FE-SEM, Model JEOL JSM 5410, Japan) with an accelerating voltage of 20 kV. The materials composed morphology was studied by a JEOL model 5300 EDS with a playback voltage of 5.0 kV. For further zeta potential calculation, Zetasizer (model: Zetasizernano ZS 90 Malvern instruments, UK) was applied. Magnetic features of $NiFe_2O_4$, Ce–$NiFe_2O_4$ and Nd–$NiFe_2O_4$ were evaluated by using vibration sample magnetometer analysis under an external magnetic field up to 20 kOe.

Catalytic procedures

The catalytic (ep)oxidation of 1,2-cyclooctene or other alkenes (1.0 mmol) was initiated by either 30% aqueous H_2O_2 (3.0 mmol) or 70% aqueous *t*-BuOOH (*tert*-butylhydroperoxide, 1.5 mmol), as an internal oxidant, fed with 0.01, 0.02, 0.05 and 0.1 g of the spiral ferrite catalyst ($NiFe_2O_4$, Ce–$NiFe_2O_4$ or Nd–$NiFe_2O_4$) in 10 mL of acetonitrile (or other given solvent) at 85 °C in an oil bath with magnetic stirring for 160 min under heterogeneous aerobic conditions. The catalytic processes were controlled by withdrawing samples (~ 1 mL) at different time intervals during the catalytic process. The withdrawal samples were collected at the desired time and treated with solid sodium thiosulfate (~ 10 mg) to quench the unreacted excess an aqueous H_2O_2 or *t*-BuOOH in the reaction media under the same conditions for each catalytic sample. The resulting slurry was filtered on celite, and the filtrate was diluted by the given solvent (1: 3) mixed in a vortex. Then, 1 μL of the filtrated sample was injected in the GC–MS.

The catalytic products were examined by Shimadzu gas chromatography mass spectrometer (GC–MS) of model QP2010 SE furnished by a capillary column of Rxi-5 Sil MS (30 m length × 0.25 mm ID × 025 um film thickness. The GC experimental conditions are 250 °C injector temperature, 40 °C initial oven temperature (held for 1 min), and then the oven temperature was increased to 200 °C with a rate of 10 °C min^{-1}. With the splitless mode, the inlet was operated. The MS transfer line was held at 200 °C. High-purity helium was the carrier gas with a flow rate of 1 mL min^{-1}. The analytical data of the compounds' percentages were determined and analyzed by LabSolution software. Peaks identification was made by comparing the mass spectra of detected compounds with NIST mass spectral library.

Result and discussion

Synthesis of $NiFe_2O_4$, Ce–$NiFe_2O_4$ and Nd–$NiFe_2O_4$

Nickel ferrite and its Ce- and Nd-doped spinel nanomaterials were prepared by using the sol–gel method forming nanopowders. The appropriated amounts of polyethylene glycol (non-ionic surfactant) and tartaric acid (dicarboxylic acid) were mixed as structure-directing templates into control of the shape and size of $NiFe_2O_4$ and its Ce- and Nd-doped spinels. Moreover, the applied synthetic route could show a significant influence on the degree of ferrite-purity, size distribution and crystallinity with less agglomeration. The characterization analyses could be conducted for all samples, which are shown below. The currently applied method for nickel ferrite and its Ce- and Nd-doped spinel nanomaterials preparation was different from the previously used ones [49, 50].

Characterization

Figure 1a shows the FTIR spectra of $NiFe_2O_4$, Ce–$NiFe_2O_4$ and Nd–$NiFe_2O_4$. A distinguished broad vibrational band was observed at 2330 cm^{-1}, which was assigned for the adsorbed CO_2. The adsorbed CO_2 was due to the residual species of the calcination process of the organic additives. The organic additives were used already in the preparation of the spiral ferrites and helped to stabilize the doped particles in the nickel ferrite. The tetrahedral and octahedral modes of $NiFe_2O_4$ were assigned by the remarkable stretching bands at 550 cm^{-1} and 448 cm^{-1}, respectively. These illustrious bands corresponded to the mutual substitution among the spinel (Ni^{2+}/Fe^{3+}oxide) tetrahedral and the octahedral (Fe^{3+}–O) sites [51].

XRD analysis of the prepared samples is presented in Fig. 1b, and the patterns were in a good agreement of the expected tetrahedral and octahedral spinal type of the face-centered cubic nickel ferrite (Ref code 01-071-3850) [52], confirming no impurities could be found. The crystalline planes were recorded at 30.2° (220), 35.3° (311), 38.5° (222), 43.2° (400), 53.6° (422), 57.2° (511), 63.2° (440), 75.5° (533) and 76.3° (622). The similarity in the XRD patterns of $NiFe_2O_4$ and its doped Ce and Nd species without any further diffraction observable peaks could be mainly owed to the successful prevention of growth, which caused a decrease in the crystallization intensity.

The crystallite size of $NiFe_2O_4$ and its doped nanomaterials was estimated by measuring the broadening of the half-width of the full maxima (HWFM) of (311) peak, which stipulated nanoscale of the prepared samples. These data were confirmed with the calculated magnitudes through Scherrer's formula [53]:

$$D = \frac{0.9\lambda}{\beta \cos \theta} \tag{1}$$

where λ is the wavelength of Cu Kα1 radiation ($\lambda = 1.54$ Å), β is the full width at half maximum of the diffraction peak, D is the crystallite size, 0.9 is a value of a shape constant, and θ is the Bragg diffraction angle. The crystallite sizes (D) were found to be 8.5, 10 and 7 nm for $NiFe_2O_4$, Ce–$NiFe_2O_4$ and Nd–$NiFe_2O_4$, respectively.

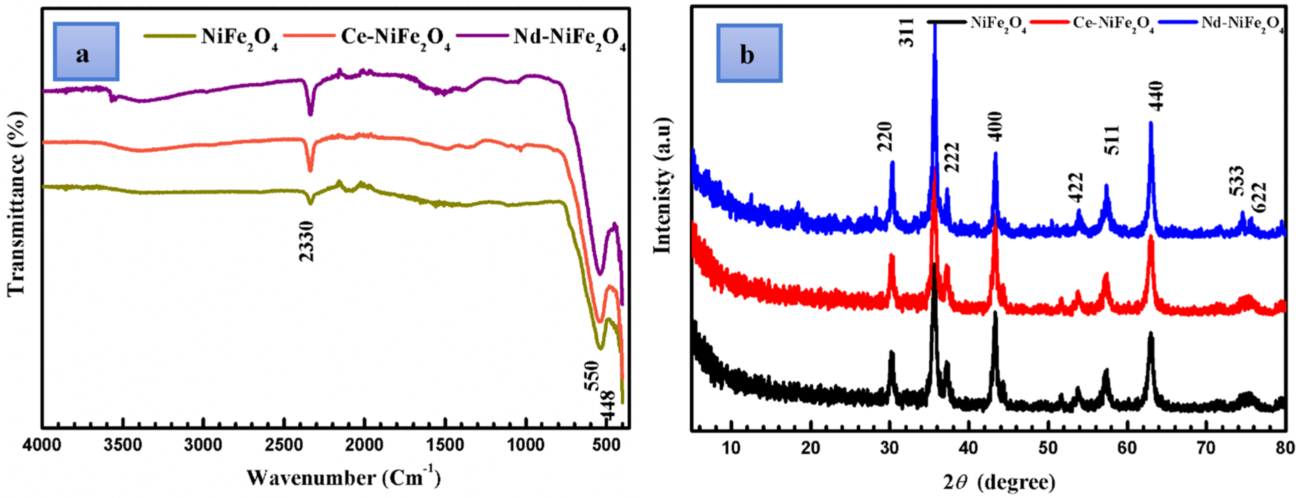

Fig. 1 FTIR spectra of $NiFe_2O_4$ and doped Ce–$NiFe_2O_4$ and Nd–$NiFe_2O_4$ nanoparticles (**a**), XRD patterns (**b**)

Figure S1 presents the zeta potential distribution of the $NiFe_2O_4$ nanoparticles, which was detected between − 25.4 and − 30.2 mV. The negative value of zeta potential could be assigned for a negative surface charge on the $NiFe_2O_4$ nanoparticles. As a consequence, it afforded a compatible description of the physiological stability and successful synthetic process of the three spinel ferrite nanomaterials.

Figure 2a describes the FE-SEM morphology of the Nd–$NiFe_2O_4$ material. From FE-SEM images, the agglomerated particles were investigated within the magnetic dipole interaction between nanoparticles and interval sizes. The estimated particle size was nearly to be 14.5–18.4 nm, which is bigger than the resulted crystallite size by XRD. Such a case could be accounted for the existence of particles as polycrystalline. Figure 2b displays the EDS analysis of the Nd–$NiFe_2O_4$ sample to confirm its elemental contents. The EDS spectrum of Nd–$NiFe_2O_4$ showed characteristic peaks corresponding to O, Fe and Ni, indicating the presence of Nd atoms in $NiFe_2O_4$ in small scale, assigning the successful synthetic process.

From TEM micrographs, the nanoferrites were semi-spherical in shape, as shown in Fig. 3a, b, c. The calculated particle sizes were so congruent with those evaluated data by XRD for the three studied materials. The particle size distributions were assigned to be 10, 11 and 8 nm for $NiFe_2O_4$, Ce–$NiFe_2O_4$, and Nd–$NiFe_2O_4$, respectively. Figure 3d of HRTEM reveals the Millar indices of {311} with the d-spacing of 0.25 nm among the adjacent planes exhibiting the growth tendency with the existence of each particle as a single crystal of $NiFe_2O_4$. The same behavior was remarked by doping $NiFe_2O_4$ with the lanthanum element (Ce or Nd). Coalescence of small particles (Ce or Nd) that occurred within $NiFe_2O_4$ should logically configure the large size of $NiFe_2O_4$, as reported previously for the coalescence of Ce-doped $BiFeO_3$ nanoflakes [54]. A typical trend was explored elsewhere for the Nd^{3+} substitution influence in the physical features of nanocrystalline nickel ferrites [55]. Therefore, in the current report, a slight decrease in particle size of $NiFe_2O_4$ was obtained due to the incorporated Ce^{3+} or Nd^{3+} ions into its crystalline lattice at the inner borders. Such a doping process could make some lattice strain, which prevented the particle growth of $NiFe_2O_4$. Furthermore, the energy was exerted in the insertion of Nd^{3+} into nickel ferrite lattice rather than particle size growth of $NiFe_2O_4$, as observed for the impact of Dy^{3+}-substituted nickel ferrite [55]. On the other hand, SAED crystal diffraction patterns clarified a bright spot surrounded by rings with different d-spacing, as shown in Fig. 3e. Those results were matched with the XRD studies and confirmed the crystalline nature of the prepared nanonickel ferrites.

The vibrating sample magnetometer (VSM) analysis displayed the magnetic characteristics of $NiFe_2O_4$, Ce–$NiFe_2O_4$ and Nd–$NiFe_2O_4$, which presented as magnetization curves in Fig. 4. The nonlinear and reversible behavior without any hysteresis loop accomplished soft ferromagnetic properties of the current nanomaterials, especially for Ce–$NiFe_2O_4$ and Nd–$NiFe_2O_4$. The magnetization magnitudes, which are derived from Fig. 4, were obtained as 28.02, 17.98 and 16.00 emu g^{-1} for $NiFe_2O_4$, Ce–$NiFe_2O_4$ and Nd–$NiFe_2O_4$, respectively. The observed dropping of the magnetization for $NiFe_2O_4$ within its doped Ce and Nd species compared to that of the free $NiFe_2O_4$ could be attributable to the incorporated nanoparticles of Ce and Nd in the nickel ferrite lattice. The decline in the magnetization from 28.02 emu g^{-1} to 17.98 and 16.00 emu g^{-1} could be enough for any further magnetic separation in the reusability of those catalysts in the (ep)oxidation protocols.

From the above characteristic studies, the polymeric and organic additives (tartaric acid) in the synthetic method showed their critical role in the doped Ce and Nd in nickel

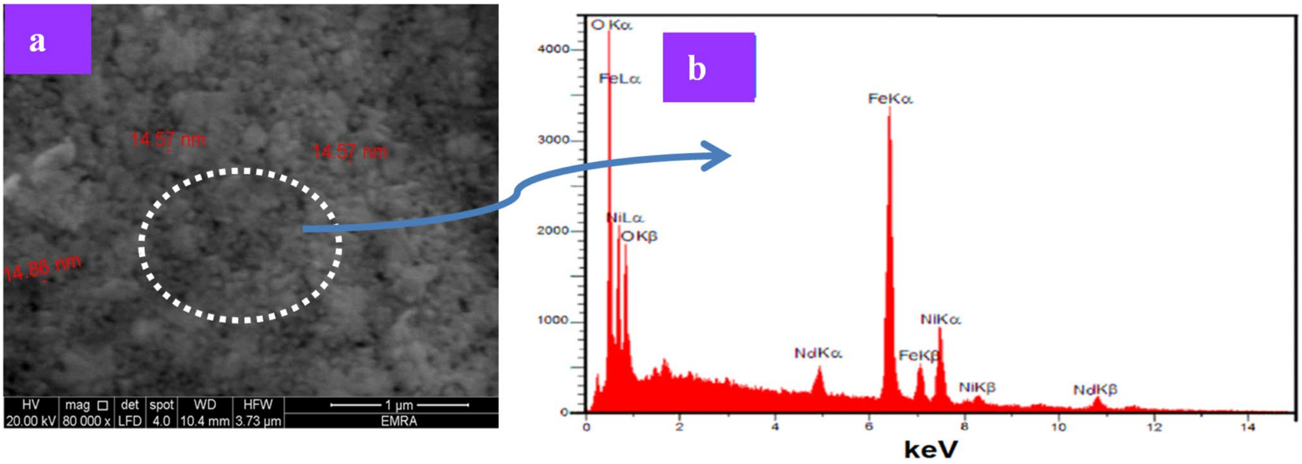

Fig. 2 FE-SEM micrograph of $NiFe_2O_4$ (**a**), EDS analysis of Nd–$NiFe_2O_4$ (**b**)

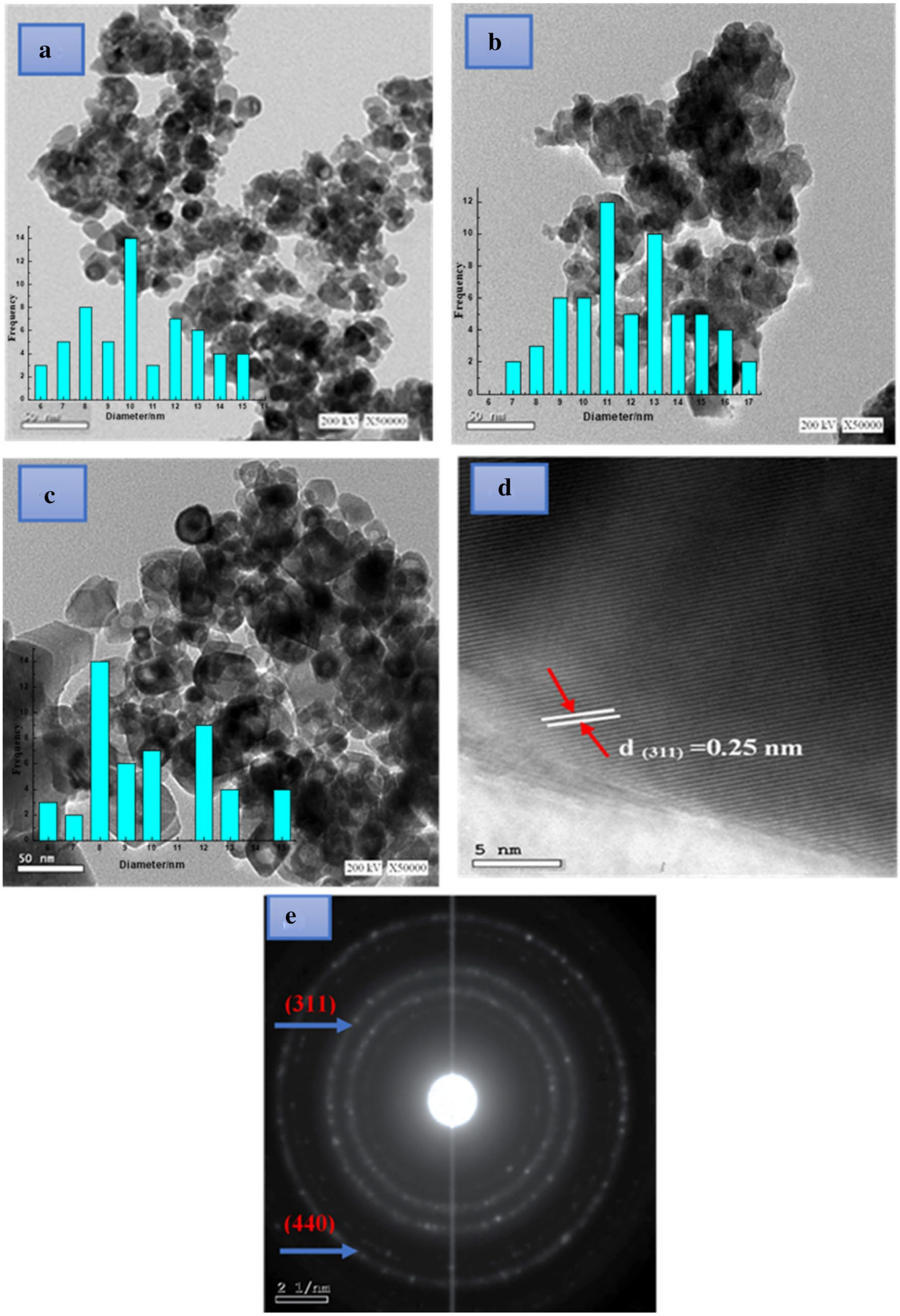

Fig. 3 TEM micrographs $NiFe_2O_4$ (**a**), Ce–$NiFe_2O_4$ (**b**), Nd–$NiFe_2O_4$ (**c**), HRTEM image (**d**) with its calculated histogram, and SAED patterns (**e**) of $NiFe_2O_4$

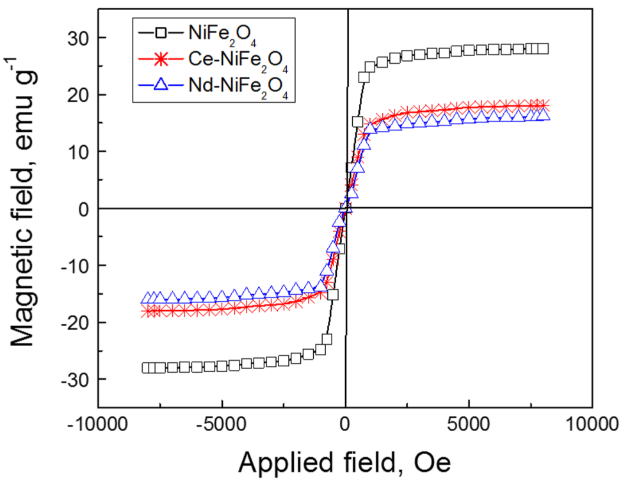

Fig. 4 Magnetic curves of $NiFe_2O_4$, Ce–$NiFe_2O_4$ and Nd–$NiFe_2O_4$

ferrite. The organic additives prevented the nanoparticle growth of nickel ferrite obviously, resulting in the well-defined and orderly formation of nickel ferrite nanoparticles at a low calcination temperature of 450 °C. As well as, the organic additives have a good action for improvement of the stability of nickel ferrite sol performing as a well-dispersed phase in PEG or the tartaric acid matrix.

Catalytic potential in (ep)oxidation of alkenes

The catalytic capacity of $NiFe_2O_4$, Ce–$NiFe_2O_4$ and Nd–$NiFe_2O_4$ was probed in the (ep)oxidation of 1,2-cyclooctene as the standard model substrate of alkenes by an aqueous H_2O_2 and *t*-BuOOH, as oxygen sources, in acetonitrile. The optimized time for the catalytic processes was examined at 85 °C with 0.10 g loaded of the heterogeneous catalyst, and the results are recorded in Table 1. The percentages of the most probable products of the catalytic (ep)oxidation of 1,2-cyclooctene, which were detected by GC–MS, are recorded in Table 1. The identified products were listed as epoxy-1,2-cyclooctane (as the main and chemoselective product), 4-cyclooctene-1-one, cyclooctane, cyclooctane-1,2-diol, 2-cyclooctene-1-one and 2-hydroxycyclooctaneone [57]. The catalytic process of 1,2-cyclooctene (ep)oxidation was not progressed in the absence of the studied catalysts at 85 °C.

Figures 5, 6 and 7 present the consumed time for the (ep)oxidation of 1,2-cyclooctene catalyzed by $NiFe_2O_4$,

Table 1 Catalytic (ep)oxidation products conversion percentages of 1,2-cyclooctene oxidation using an aqueous H_2O_2 or TBHP catalyzed by $NdNiFe_2O_4$, $CeNiFe_2O_4$ and $NiFe_2O_4$ at 85 °C for in acetonitrile

Catal.[a]	Time (min.)	Conversion (%)		Product selectivity (%)											
		1,2-Cyclooctene		Epoxy-1,2-cyclooctane 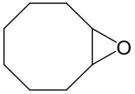		4-Cyclooctene-1-one 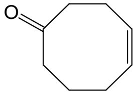		Cyclooctanone 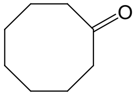		Cyclooctane-1,2-diol 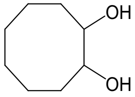		2-Cyclooctene-1-one 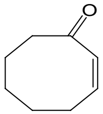		2-Hydroxycyclooctanone 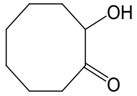	
		H_2O_2	TBHP	H_2O_2	TBHP	H_2O_2	TBHP	H_2O_2	TBHP	H_2O_2	TBHP	H_2O_2	TBHP	H_2O_2	TBHP
Nd–$NiFe_2O_4$	30	19.9	52.4	76.4	50.6	4.6	5.5	1.9	7.2	2.7	6.6	8.2	25.1	6.3	4.9
	60	29.1	57.8	64.5	48.7	4.2	4.8	5.2	6.6	11.1	5.6	6.8	29.1	8.2	5.1
	90	37.9	57.5	69.1	52.6	4.6	5.1	3.0	6.8	10.5	5.8	6.9	23.8	6.0	5.9
	120	42.9	83.8	69.4	49.5	5.1	5.2	3.5	5.1	8.7	5.0	6.8	30.8	6.5	4.5
	150	64.6	94.6	60.6	53.7	5.3	6.4	3.5	6.0	13.4	5.5	7.1	21.7	10.1	6.8
Ce–$NiFe_2O_4$	30	25.0	50.6	52.2	48.3	9.1	5.0	5.4	6.1	2.5	6.1	10.5	30.7	20.2	3.8
	60	28.7	54.8	48.0	48.0	8.2	4.7	4.4	6.3	3.6	5.2	10.7	31.6	25.1	4.3
	90	35.0	59.3	64.5	53.1	7.2	7.4	5.1	6.1	3.1	7.9	9.1	24.0	11.0	1.5
	120	38.6	93.6	66.3	54.2	6.1	6.1	4.4	6.4	3.3	4.0	7.9	26.8	11.9	2.5
	150	48.8	94.8	56.4	49.9	7.5	6.1	4.8	5.2	3.3	6.4	9.9	23.4	18.1	9.0
$NiFe_2O_4$	30	35.6	48.6	52.5	41.8	9.2	5.7	4.8	6.8	8.5	7.5	8.1	33.9	16.9	4.3
	60	51.2	59.6	51.1	44.6	7.5	4.4	4.8	6.0	10.9	6.0	5.8	34.6	19.9	4.5
	90	52.1	93.8	48.2	48.8	7.3	5.3	4.5	4.9	10.9	4.4	7.5	27.3	21.7	9.3
	120	59.4	96.1	48.4	44.4	8.6	7.0	4.9	5.1	11.8	7.2	6.3	28.4	20.0	7.9
	150	79.4	96.1	41.4	40.2	7.4	4.0	3.6	4.8	11.0	6.0	7.6	29.2	29.0	15.8

[a] (Ep)oxidation of 1,2-cyclooctene (1.0 mmol) by an aqueous H_2O_2 (3.0 mmol) or TBHP (1.7 mmol), catalyst (0.10 g) in 10 mL solvent for 150 min

Ce–$NiFe_2O_4$ and Nd–$NiFe_2O_4$, respectively. With a short time of the catalytic protocol catalyzed by Nd–$NiFe_2O_4$, Ce–$NiFe_2O_4$ or $NiFe_2O_4$, the yield of the chemoselective product was low. Prolongation of the reaction time from 60, 90, 120 to 150 min, the yield was improved remarkably and gradually to the optimized amount of the formed chemoselective with all catalysts affording excellent conversion with *t*-BuOOH (~95, 95 and 96%, catalyzed by Nd–$NiFe_2O_4$, Ce–$NiFe_2O_4$ and $NiFe_2O_4$, respectively). But, with an aqueous H_2O_2, the conversion was good giving 65, 49 and 80% with Nd–$NiFe_2O_4$, Ce–$NiFe_2O_4$ and $NiFe_2O_4$, respectively (Table 1). Longer time, i.e., more than 150 min, caused fixing in the conversion with reducing in the amount of the epoxy product with an enhancement of the other side product amounts, due probably to the further (ep)oxidation of epoxy-1,2-cyclooctane with the excess amount of the oxidant [44].

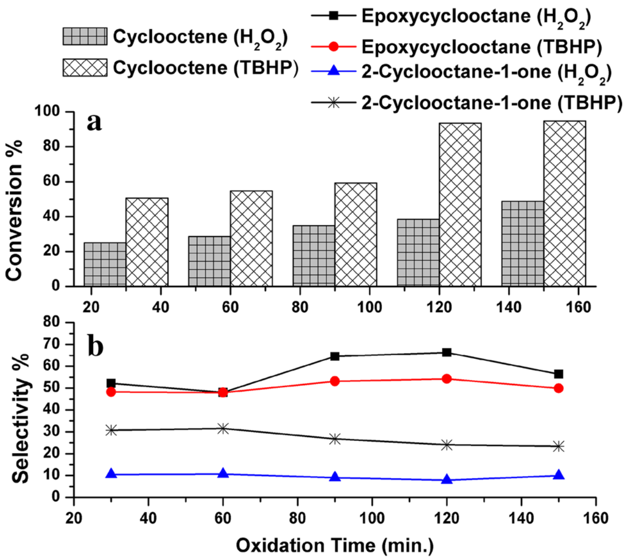

Fig. 6 Catalytic (ep)oxidation of 1,2-cyclooctene using Ce–$NiFe_2O_4$. The conversion percentages of 1,2-cylooctene presented in plot A; the product selectivity percentage of epoxy-1,2-cyclooctane and 2-cyclooctane-1-one presented in plot B, with aqueous H_2O_2 or TBHP at 85 °C as a function of time

However, the high loaded amount of the catalysts (0.10 g) was catalyzed the (ep)oxidation process, the low yield and selectivity of the welcomed epoxy product were observed (Table 1). Accordingly, new tests of the (ep)oxidation of 1,2-cyclooctene were studied with low loaded amounts of the heterogeneous catalysts (0.01, 0.02 and 0.05 g) in order to improve the yield percentages of the desired product. Table 2 assigns the various loaded amount of the Nd–$NiFe_2O_4$, Ce–$NiFe_2O_4$ or $NiFe_2O_4$ to the reaction system compared to that of the results in Table 1. The low amount of the catalysts (0.01 g) afforded very low catalytic reactivity dramatically, whereas the increased amount, i.e., 0.02 g, enhanced the yield percentage at the optimal reaction conditions. The best-inserted amount of the catalysts ($NiFe_2O_4$, Ce–$NiFe_2O_4$ and $NiFe_2O_4$) was reported with 0.05 g, which gave excellent yield percentages of epoxy-1,2-cyclooctane, 94, 90 and 87%, respectively, with *t*-BuOOH. The yield amount of the wanted product was less than that within *t*-BuOOH when an aqueous H_2O_2 was used as the oxidant. The yields were good with $NiFe_2O_4$, Ce–$NiFe_2O_4$ and $NiFe_2O_4$ awarding 83, 88 and 73%, respectively (Table 2).

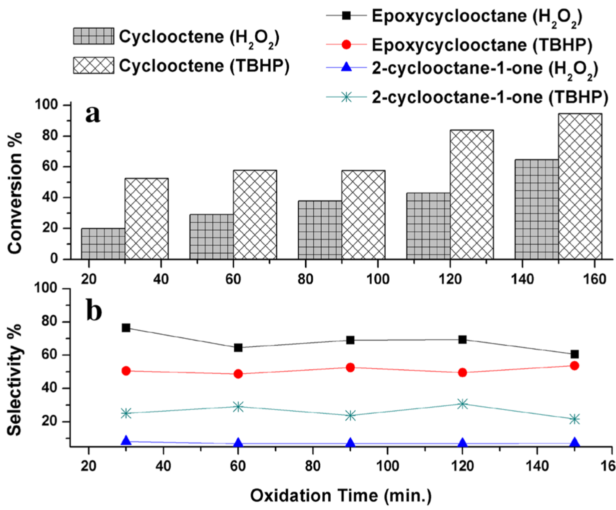

Fig. 5 Catalytic (ep)oxidation of 1,2-cyclooctene using $NiFe_2O_4$. The conversion percentages of 1,2-cylooctene presented in plot A; the product selectivity percentage of epoxy-1,2-cyclooctane and 2-cyclooctane-1-one presented in plot B, with aqueous H_2O_2 or TBHP at 85 °C as a function of time

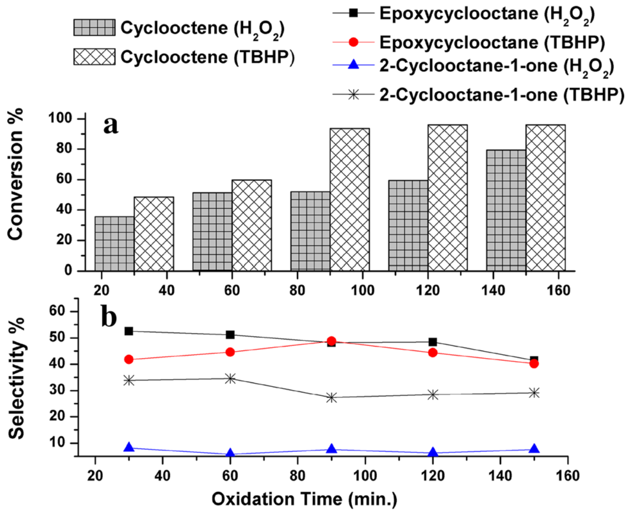

Fig. 7 Catalytic (ep)oxidation of 1,2-cyclooctene using Nd–$NiFe_2O_4$. The conversion percentages of 1,2-cylooctene presented in plot A; the product selectivity percentage of epoxy-1,2-cyclooctane and 2-cyclooctane-1-one presented in plot B, with aqueous H_2O_2 or TBHP at 85 °C, as a function of time

Table 2 Catalytic (ep)oxidation products conversion percentages of 1,2-cyclooctene oxidation using an aqueous H_2O_2 or TBHP catalyzed by $NdNiFe_2O_4$, $CeNiFe_2O_4$ and $NiFe_2O_4$ at 85 °C for with different loaded amounts in acetonitrile

Catalyst[a]	Amount of catalyst (g)	Amount of the Epoxy-1,2-cyclooctane		Conversion (%)		Selectivity (%)			
						Epoxy-1,2-cyclooctane		Other products[c]	
		H_2O_2	TBHP	H_2O_2	TBHP	H_2O_2	TBHP	H_2O_2	TBHP
Nd–$NiFe_2O_4$	0.01	30	45	40	52	75	86	25	14
	0.02	47	72	73	86	64	83	36	17
	0.05	83	94	93	100	89	94	11	6
	0.10	40	52	65	95	61	54	39	46
Ce–$NiFe_2O_4$	0.01	29	40	41	50	70	80	30	20
	0.02	46	69	69	84	66	82	34	18
	0.05	88	90	96	100	90	92	10	8
	0.10	28	48	49	95	57	50	43	50
$NiFe_2O_4$	0.01	27	36	39	48	69	75	31	25
	0.02	40	62	58	77	69	80	31	20
	0.05	73	87	89	98	82	89	18	11
	0.10	32	38	79	96	41	40	59	60

[a] (Ep)oxidation of 1,2-cyclooctene (1.0 mmol) by an aqueous H_2O_2 (3.00 mmol) or TBHP (1.7 mmol) in 10 mL acetonitrile for 150 min

t-BuOOH is reported here as an excellent oxidizing agent for the conversion and selectivity (with 0.05 g of the catalyst) of 1,2-cyclooctene catalyzed by Nd–$NiFe_2O_4$, Ce–$NiFe_2O_4$ and $NiFe_2O_4$ compared that with the aqueous H_2O_2. The rich amount of water with H_2O_2 molecules could vigorously compete with H_2O_2 molecules to bond to the catalyst and so impeded the electron and oxygen transfer processes in the catalytic system [57]. Moreover, water molecules could occupy the active sites on the surface of the probed catalysts, so water could reduce the catalytic activity of the ferrite catalysts by aqueous hydrolysis [42, 58].

On the other hand, *t*-BuOOH presented lower selectivity percentages, i.e., lower amounts of the epoxy product, compared to that with aqueous H_2O_2 (when 0.10 g used of the catalysts). The internal alcoholysis of the oxidation product of *t*-BuOOH, i.e., *tert*-BuOH, could carry out for the epoxy product percentages, as reported elsewhere [59]. This could explain the large loaded amount of the catalysts that cause the opposite behavior. In reality, the low loaded amounts of the catalysts could prevent such a phenomenon of the oxidant, i.e., *t*-BuOOH.

The second detected formed product, after the selective epoxy-1,2-cyclooctene (for 0.10 g of the loaded catalysts, Table 1), was different according to the type of oxidant. With *t*-BuOOH, the second percentage of the product was 2-cyclooctene-1-one catalyzed by Nd–$NiFe_2O_4$, Ce–$NiFe_2O_4$ and $NiFe_2O_4$ with percentages 22, 23 and 29%, respectively, after 150 min. The amounts of 2-cyclooctene-1-one were very high at 60 after 90 and 120 min (Table 1). With an aqueous H_2O_2, the second formed product was 2-hydroxycyclooctanone with percentages 10, 18 and 29% yields catalyzed by Nd–$NiFe_2O_4$, Ce–$NiFe_2O_4$ and $NiFe_2O_4$, respectively. The high formed amounts of 2-hydroxycyclooctanone with an aqueous H_2O_2 could be resulted from the presence of a high amount of water of the aqueous H_2O_2 in the reaction media causing, probably an aqueous hydrolysis of the chemoselective product [58].

Effect of solvent

Various solvents, e.g., ethanol, acetone, chloroform, 1,2-dichloroethane and dimethyl sulfoxide (DMSO), were applied to investigate the catalytic activity of Nd–$NiFe_2O_4$, Ce–$NiFe_2O_4$ and $NiFe_2O_4$ in the (ep)oxidation of 1,2-cyclooctene by an aqueous H_2O_2 or *t*-BuOOH. The percentages of conversion and selectivity are listed in Table 3. Among the studied solvents, chloroform and 1,2-dichloroethane were found to be better than acetonitrile, ethanol, acetone and DMSO for those catalytic systems at the optimized conditions (150 min and 85 °C), which gave the maximum conversion and epoxy selectivity percentages with both oxidants (H_2O_2 and *t*-BuOOH) (Table 3).

The high power of coordination ability of acetonitrile, ethanol and acetone could have strong competition with the oxidant (H_2O_2 or *t*-BuOOH) to coordinate to the metal ion of the catalyst within occupying the active coordination sites on the catalyst surface [46, 48]. This could explain why the catalytic reactivity of the current catalysts was reduced in those polar solvents compared to those solvents with less coordination ability (chloroform and dichloromethane). Moreover, the high coordination capability of DMSO could diminish the catalytic efficiency of the studied catalyst materials, due to the high probability of DMSO to coordinate to the central metal ion of Nd–$NiFe_2O_4$, Ce–$NiFe_2O_4$ and $NiFe_2O_4$.

Table 3 Catalytic (ep)oxidation products conversion percentages of 1,2-cyclooctene oxidation using an aqueous H_2O_2 or TBHP catalyzed by $NdNiFe_2O_4$, $CeNiFe_2O_4$ and $NiFe_2O_4$ at 85 °C in different solvents

Catalyst[a]	Solvent	Conversion (%)		Selectivity (%)			
				Epoxy-1,2-cyclooctane		Other products[c]	
		H_2O_2	TBHP	H_2O_2	TBHP	H_2O_2	TBHP
Nd–$NiFe_2O_4$	Acetonitrile	65	95	61	54	39	46
	Ethanol	63	91	58	50	42	50
	Acetone	59	89	55	48	45	52
	Chloroform	85	97	84	68	16	32
	Dichloromethane	84	95	81	65	19	35
	DSMO	79	88	54	44	46	56
Ce–$NiFe_2O_4$	Acetonitrile	49	95	57	50	43	50
	Ethanol	48	90	51	45	49	55
	Acetone	48	88	44	41	56	59
	Chloroform	82	90	81	65	19	35
	Dichloromethane	78	84	76	60	24	40
	DSMO	72	79	51	42	49	58
$NiFe_2O_4$	Acetonitrile	79	96	41	40	59	60
	Ethanol	65	90	40	39	60	61
	Acetone	61	87	35	34	65	66
	Chloroform	82	87	71	56	29	44
	Dichloromethane	79	81	67	51	33	49
	DSMO	68	78	46	37	54	63

[a] (Ep)oxidation of 1,2-cyclooctene (1.0 mmol) by an aqueous H_2O_2 (3.00 mmol) or TBHP (1.7 mmol), catalyst (0.10 g) in 10 mL solvent for 150 min

Additionally, low polarity and high covalence properties of chloroform and 1,2-dichloroethane compared to acetonitrile, ethanol and acetone interpreted the low polarity of the reaction system, i.e., the reaction could probably take place with electron parking mechanism [60, 61]. The most common mechanistic pathway of such (ep)oxidation reaction progresses within electron and oxygen transfer processes [61], and the low polar solvents are the best reaction media. This phenomenon has been observed previously [46, 62].

Effect of type of catalysts

The homogeneous or heterogeneous inorganic catalytic processes depend mainly on the type and charge of the central metal ion in its material [63, 64]. However, $NiFe_2O_4$ showed the highest conversion of 1,2-cyclooctene (ep)oxidation compared to those Nd–$NiFe_2O_4$ and Ce–$NiFe_2O_4$ (Figs. 5, 6, 7), and it awarded the lowest catalytic selectivity with both *t*-BuOOH and H_2O_2 (40 and 41%, respectively) (Table 1). Hence, the presence of the Nd- or Ce-doped species in nickel ferrite showed a somewhat influence on the catalytic potential of $NiFe_2O_4$, especially in the selectivity. Both doped Ce– and Nd–$NiFe_2O_4$ reduced the particle size of $NiFe_2O_4$ (10, 11 and 8 nm for $NiFe_2O_4$, Ce–$NiFe_2O_4$, and Nd–$NiFe_2O_4$) with an improvement of their surface areas, as observed by the above characterization results. This could probably promote their chemoselectivity of 1,2-cyclooctene (ep)oxidation compared to that of the free $NiFe_2O_4$. The doping of nickel ferrite with Nd or Ce as a lanthanide element enriches slightly the catalytic potential of $NiFe_2O_4$ toward the (ep)oxidation of 1,2-cyclooctene. The various oxidation number interchange and the high Lewis acid feature [65–67] of the central metal ion in the catalyst could strongly force the catalytic potential of the considered catalyst in such (ep)oxidation processes [58, 68]. This could not be taken place easily with the doped Nd and Ce, as lanthanides or f-block elements [69], with the electron and/or oxygen transfer processes in the catalytic cycles [61, 70]. Additionally, the presence of Nd or Ce in nickel ferrite increased the heterogeneous nature of nickel ferrite and so might reduce its progressing of their reactivity (Figs. 5, 6, 7) [71].

The coordination chemical feature of the central metal in the catalyst toward the oxidant and the substrate could play notably a major action in its catalytic affectivity within the electron and/or oxygen transfer processes to cause (ep)oxidation of the substrate [29]. Such a system could not be touched with lanthanides, i.e., Ce and Nd, as rare earth elements [24, 69]. Particularly, the low coordination capability of the doped Ce and Nd (as lanthanide elements), compared to the transition element, i.e., Ni and Fe in $NiFe_2O_4$ toward the oxidizing agent and the substrate could be a considerable reason for the less observable enhancement in the catalytic potential of $NiFe_2O_4$ [20–26, 72].

Although Ce and Nd have low coordination chemical behavior, the catalytic selectivity was enhanced of doped Ce– and Nd–$NiFe_2O_4$ nanospecies by increasing the yield of the epoxy product. The reason is that the surface area of nickel ferrite was enhanced by the doped Ce and Nd. Furthermore, Nd could progress the catalytic affectivity of $NiFe_2O_4$, as Nd–$NiFe_2O_4$, more than that in the presence of Ce in Ce–$NiFe_2O_4$ within the development of the active sites on the surface of nickel ferrite [73]. The particle size of the nanoparticles of nickel ferrite was decreased remarkably with the doping of Nd more than that with Ce, as reported form the XRD and TEM obtains. So, this could promote the catalytic active sites on the surface of nickel ferrite toward homogeneity [74].

(Ep)oxidation of other aliphatic and cyclic alkenes

The catalysts screening for the (ep)oxidation of various alkenes within cyclic and acyclic chains at the optimization was studied, and the obtained results are recorded in Table 4. All catalysts were efficiently capable of catalyzing the (ep)oxidation of those alkenes to their corresponding epoxy products by an aqueous H_2O_2 or *t*-BuOOH. Cyclic alkenes, e.g., 1,2-cyclooctene, 1,2-cyclohexene and styrene with higher electron-donating power by the C=C double bond estimated an (ep)oxidation reactivity more than that of the acyclic or aliphatic alkenes (Table 4) [75, 76]. Such behavior could be resulted from the inner double bonding in the cyclic alkenes compared to the terminal double bonding in the aliphatic alkenes. Type of double bonding of alkene might influence the coordination to the central metal ion of the catalyst and so could affect the reactivity of the alkene toward the (ep)oxidation [46].

Recyclability

The recyclability of the novel catalysts was registered with repeating of the (ep)oxidation of 1,2-cyclooctene with *t*-BuOOH at the optimum reaction conditions, magnetically (Table 5). The easy extraction of the catalysts was accomplished by a magnet for further catalytic tests. In particular, Nd–$NiFe_2O_4$, Ce–$NiFe_2O_4$ and $NiFe_2O_4$ showed high catalytic reactivity for 5 times of recycling experiments with long-time durability.

After 6 times of the recycling, the new catalysts presented a remarkable loss of their potential was almost 20%, as shown in Table 5. The reason for the deactivation of the catalysts could be considered as the diminution of the active sites and the active centers. Figure 8 presents the EDS analyses of the reused of Nd–$NiFe_2O_4$ after 6 times, representatively, as observed elsewhere [77]. Clearly, there was no considered change in the morphology of Nd–$NiFe_2O_4$ to lose its catalytic potential. So, there is no obvious reason for

Table 4 (Ep)oxidation of some cyclic and acyclic alkenes catalyzed by Nd–$NiFe_2O_4$, Ce–$NiFe_2O_4$ and $NiFe_2O_4$ using an aqueous H_2O_2 or TBHP

Entry	Alkene[a]	Product	Conversion, % (Selectivity, %)					
			$NdNiFe_2O_4$		$CeNiFe_2O_4$		$NiFe_2O_4$	
			H_2O_2	TBHP	H_2O_2	TBHP	H_2O_2	TBHP
1	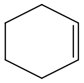	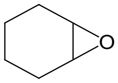	87 (85)	96 (72)	85 (81)	92 (70)	82 (83)	88 (60)
2	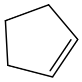	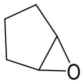	80 (75)	89 (69)	77 (70)	88 (68)	77 (69)	79 (60)
3	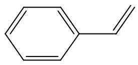	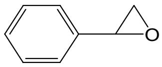	84 (78)	90 (74)	81 (76)	88 (71)	78 (67)	78 (63)
4	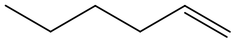	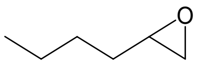	71 (58)	81 (56)	67 (53)	74 (52)	62 (49)	61 (45)
5	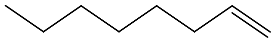	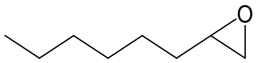	64 (49)	71 (49)	52 (42)	65 (41)	48 (38)	54 (40)
6	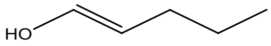	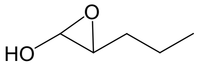	88 (45)	85 (43)	79 (41)	80 (39)	72 (29)	77 (37)

[a]Reaction carried out in chloroform (10 mL), alkene (1.0 mmol), H_2O_2 (3.0 mmol) or TBHP (1.7 mmol) and catalyst (0.10 g) at 85 °C after 150 min

Table 5 Number of recycling of the catalysts (Nd–$NiFe_2O_4$, Ce–$NiFe_2O_4$ and $NiFe_2O_4$) in the (ep)oxidation of 1,2-cyclooctene by an aqueous H_2O_2 and TBHP

No. of recycling[a]	Conversion, % (Selectivity, %)					
	$NdNiFe_2O_4$		$CeNiFe_2O_4$		$NiFe_2O_4$	
	H_2O_2	TBHP	H_2O_2	TBHP	H_2O_2	TBHP
1	85 (84)	97 (68)	82 (81)	90 (65)	82 (71)	87 (56)
2	85 (84)	97 (68)	82 (80)	90 (65)	82 (71)	87 (55)
3	83 (84)	95 (68)	82 (80)	89 (65)	82 (69)	87 (55)
4	83 (82)	95 (68)	82 (79)	89 (65)	82 (69)	85 (55)
5	82 (81)	91 (68)	80 (80)	87 (65)	80 (67)	84 (54)
6	75 (70)	84 (48)	71 (59)	62 (47)	58 (49)	58 (39)

[a] Reaction carried out in chloroform (10 mL), 1,2-cyclooctene (1.0 mmol), H2O2 (3.0 mmol) or TBHP (1.7 mmol) and catalyst (0.10 g) at 85 °C after 150 min

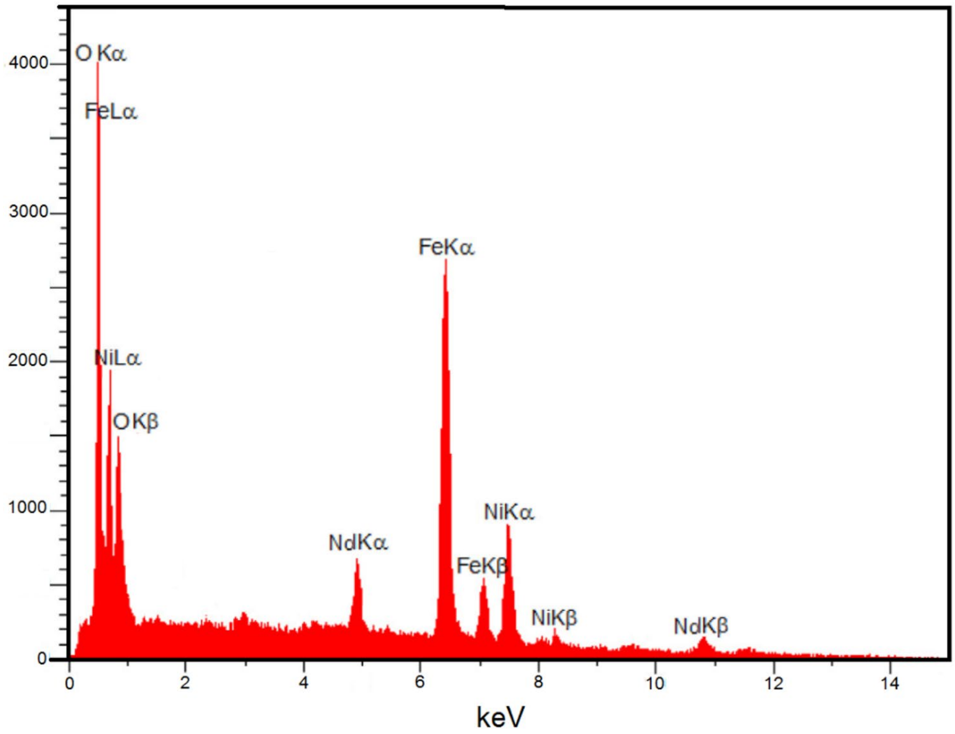

Fig. 8 EDS analysis of Nd–$NiFe_2O_4$ after the recycling of the (ep)oxidation of 1,2-cyclooctene with aqueous H_2O_2

its deactivation, which could be found elsewhere or could explain that behavior.

Overall possible mechanism

A representative mechanism of 1,2-cyclooctene (ep)oxidation could be displayed within current catalysts of $NiFe_2O_4$ and its doped Ce and Nd nanoparticles, as mixed spinel structures. A fast electron exchange between M^{2+} and M^{3+} ions occurred (electron transfer process) of Nd–$NiFe_2O_4$, Ce–$NiFe_2O_4$ and $NiFe_2O_4$ [78]. $NiFe_2O_4$ and its doped were oxidized with H_2O_2 or *t*-BuOOH and through the changes of Fe^{2+} and Ni^{3+} to Fe^{3+} and Ni^{2+} ions (within the electron transfer process), respectively, generate and OH^- or *t*BuO^- anions [79]. The liberating of OH^- or *t*BuO^- anions was accomplished by proton transmission from H_2O_2 or *t*-BuOOH molecule to the oxygen atom of the spinel ferrite catalyst. A generation of OH^- anion with Lewis acidic center of the metal in spinel ferrites could subsequently react with alkene C=C double bond to give the epoxy product in good yields (within the oxygen transfer process) [24]. Then, the leaving catalyst could start a new catalytic cycle.

The selectivity of the spinel ferrite catalysts toward the (ep)oxidation processes is based upon the distribution of the cation ions of the dopant Ce and Nd ions in octahedral Oh sites [80]. This could be discussed as the catalyst active centers in the octahedral active sites, which mainly localized at the spinel ferrite surface. Significantly, Nd–$NiFe_2O_4$ showed slightly more selectivity toward the (ep)oxidation of 1,2-cyclooctene, as interpreted above.

Conclusions

Free nickel ferrite and its doped Ce–$NiFe_2O_4$ and Nd–$NiFe_2O_4$ nanoparticles were successfully synthesized through the sol–gel route. The physicochemical characterizations including FTIR, XRD, FE-SEM, TEM, SAED and EDS were investigated to distinguish the morphology, chemical bonds, crystallinity and chemical analyses of the fabricated $NiFe_2O_4$, Ce–$NiFe_2O_4$ and Nd–$NiFe_2O_4$. The XRD patterns emphasized the existence of the tetrahedral and octahedral spinel-type of nickel ferrite for all samples without any further impurities. The obtained crystallite sizes were estimated as 8.5, 10 and 7 nm for $NiFe_2O_4$, Ce–$NiFe_2O_4$ and Nd–$NiFe_2O_4$, respectively. SAED patterns emphasized the crystalline nature of the prepared nanomaterials. FE-SEM images illustrated the uniform and homogenous distribution of Nd–$NiFe_2O_4$ nanoparticles by an average size of 14.5–18.4 nm. All catalysts show excellent conversion with *t*-BuOOH at 85 °C (~ 95, 95 and 96%, catalyzed by Nd–$NiFe_2O_4$, Ce–$NiFe_2O_4$ and $NiFe_2O_4$, respectively) after 150 min in the (ep)oxidation of 1,2-cyclooctene. With all catalysts, *t*-BuOOH showed higher oxidation influence on the conversion of 1,2-cyclooctene than that with an aqueous H_2O_2. With *t*-BuOOH, the catalytic system afforded lower chemoselectivity due to the alcoholysis effect with the high loaded amounts of the catalysts (0.10 g). But, with lower loaded amount of the catalysts (0.05 g), the catalytic activity of Nd–$NiFe_2O_4$, Ce–$NiFe_2O_4$ and $NiFe_2O_4$ was optimized to give an excellent yield of the epoxy product. Cyclic alkenes awarded higher conversion and selectivity more than the acyclic alkenes. Doping of Nd and Ce enhanced the ion ratio at the octahedral Oh sites and hence enhanced their activity and selectivity toward the alkenes (ep)oxidation. The reusability of the magnetic catalysts was probed and exhibited a maximum 5 times of catalyst cycling under the easy separation by exposing to an external magnet. This systematic report introduces novel nanocatalysts Nd–$NiFe_2O_4$ and Ce–$NiFe_2O_4$ toward the alkenes (ep)oxidation.

Acknowledgements The authors acknowledge the Deanship of Scientific Research at King Faisal University for the financial support under the annual research project (Grant No. 180074).

References

1. T. Tolaymat, A. El Badawy, A. Genaidy, W. Abdelraheem, R. Sequeira, J. Clean. Prod. **143**, 401 (2017)
2. K. Ueda, M. Tsuji, J. Ohyama, A. Satsuma, ACS Catal. **9**, 2866 (2019)
3. G. Kaur, P. Devi, S. Thakur, A. Kumar, R. Chandel, B. Banerjee, ChemistrySelect **4**, 2181 (2019)
4. W. Wang, D. Zhang, RSC Adv. **8**, 32221 (2018)
5. W. Zhang, Y. Xu, H. Wang, C. Xu, S. Yang, Sol. Energy Mater. Sol. Cells **95**, 2880 (2011)
6. N. Senthilkumar, M. Pannipara, A.G. Al-Sehemi, G.G. Kumar, New J. Chem. **43**, 7743 (2019)
7. K.M. Reddy, L. Satyanarayana, S.V. Manorama, D.K. Misra, Mater. Res. Bull. **39**, 1491 (2003)
8. A.P. Alivisatos, Science **271**, 933 (1996)
9. M. Junaid, M.A. Khana, M.N. Akhtar, A. Hussain, M.F. Warsi, Ceram. Int. **45**, 13431 (2019)
10. A.A. Ensafi, A.R. Allafchian, Colloids Surface B **102**, 687 (2013)
11. S. Payra, A. Saha, S. Banerjee, RSC Adv. **6**, 52495 (2016)
12. A. Sheoran, M. Dhiman, S. Bhukal, R. Malik, J. Agarwal, B. Chudasama, S. Singhal, Mater. Chem. Phys. **222**, 207 (2019)
13. X. Guo, D. Wang, J. Environ. Chem. Eng. **7**, 102814 (2019)
14. B. Behdadfar, A. Kermanpur, H. Sadeghi-Aliabadi, Molares M. del Puerto, M. Mozaffari, J. Solid State Chem. **187**, 20 (2012)
15. A.K. Gupta, M. Gupta, Biomaterials **26**, 3995 (2005)
16. S. Mosivand, I. Kazeminezhad, Ceram. Int. **41**, 8637 (2015)
17. A. Javidan, S. Rafizadeh, S.M. Hosseinpour-Mashkani, Mater. Sci. Semicond. Process. **27**, 468 (2014)
18. M. Hashim, K.S. Alimuddin, B.H. Koo, S.E. Shirsath, E.M. Mohammed, J. Shah, R.K. Kotnala, H.K. Choi, H. Chung, R. Kumar, J. Alloys Compd. **518**, 11 (2012)
19. K.V. Babu, G.V.S. Kumar, K. Jalaiah, P.T. Shibeshi, J. Phys. Chem. Solids **118**, 172 (2018)
20. E. Uyanga, D. Sangaa, H. Hirazawa, N. Tsogbadrakh, N. Jargalan, I.A. Bobrikov, A.M. Balagurov, J. Mol. Struct. **1160**, 447 (2018)
21. B.I. Kharisov, H.V.R. Dias, O.V. Kharissova, Arab. J. Chem. **12**, 1234 (2019)
22. R. Galindo, E. Mazario, S. Gutiérrez, M.P. Morales, P. Herrasti, J. Alloys Compd. **536S**, S241 (2012)
23. R. Galindo, S. Gutiérrez, N. Menéndez, P. Herrasti, J. Alloys Compd. **586**, S511 (2014)
24. A.M. Kulkarni, U.V. Desai, K.S. Pandit, M.A. Kulkarni, P.P. Wadgaonkar, RSC Adv. **4**, 36702 (2014)
25. R. Saranya, R.A. Raj, M.S. AlSalhi, S. Devanesan, J. Supercond. Nov. Magn. **31**, 1219 (2018)
26. I.T. Cunha, I.F. Teixeira, A.S. Albuquerque, J.D. Ardisson, W.A.A. Macedo, H.S. Oliveira, J.C. Tristão, K. Sapage, R.M. Lago, Catal. Today **259**, 222 (2015)
27. J. He, S. Yang, A. Riisager, Catal. Sci. Technol. **8**, 790 (2018)
28. A. Goyal, S. Kapoor, P. Samuel, S. Singhal, Anal. Chem. Lett. **6**, 98 (2016)
29. P. Samoila, C. Cojocaru, L. Sacarescu, P.P. Dorneanu, A.-A. Domocos, A. Rotaru, Appl. Catal. B **202**, 21 (2017)
30. N. Velinov, T. Petrova, R. Ivanova, T. Tsoncheva, D. Kovacheva, I. Mitov, Hyperfine Interact. **241**, 31 (2020)
31. Y. Choi, B.S. Seong, S.S. Kim, Phys. B **404**, 689 (2009)
32. M. Chithra, C.N. Anumol, B. Sahu, S.C. Sahoo, J. Magn. Magn. Mater. **401**, 1 (2016)
33. J. Zhou, J. Ma, C. Sun, L. Xie, Z. Zhao, H. Tian, Y. Wang, J. Tao, X. Zhu, J. Am. Ceram. Soc. **88**, 3535 (2005)
34. Y. Wang, L. Li, J. Jiang, H. Liu, H. Qiu, F. Xu, React. Funct. Polym. **68**, 1587 (2008)
35. S. Thakur, S.C. Katyal, M. Singh, J. Magn. Magn. Mater. **321**, 1 (2009)
36. J. Wang, T. Deng, Y. Lin, C. Yang, W. Zhan, J. Alloys Compd. **450**, 532 (2008)
37. P.E. Meskin, V.K. Ivanov, A.E. Barantchikov, B.R. Churagulov, Y.D. Tretyakov, Ultrason. Sonochem. **13**, 47 (2006)
38. A. Katelnikovas, J. Barkauskas, F. Ivanauskas, A. Beganskiene, A. Kareiva, J. Sol-Gel Sci. Technol. **41**, 193 (2007)
39. J.D. Mackenzie, E.P. Bescher, Acc. Chem. Res. **40**, 810 (2007)
40. X. Zhao, Y. Wang, W. Feng, H. Lei, J. Li, RSC Adv. **7**, 52738 (2017)

41. F. Yan, K. Han, G. Zhao, X. Shi, N. Song, Z. Jiao, Mater. Charact. **124**, 90 (2017)
42. M.F.I. Al-Hussein, M.S.S. Adam, Appl. Organometal. Chem. **34**, e5598 (2020)
43. M.S.S. Adam, Appl. Organometal. Chem. **32**, e4234 (2018)
44. M.S.S. Adam, A.D.M. Mohamad, Polyhedron **151**, 118 (2018)
45. J. Li, H. Gao, L. Tan, Y. Luan, M. Yang, Eur. J. Inorg. Chem. **30**, 4906 (2016)
46. F.M. Golkhatmi, B. Bahramian, M. Mamarabadi, Mater. Sci. Eng. C **78**, 1 (2017)
47. D.T. Bregante, N.E. Thornburg, J.M. Notestein, D.W. Flaherty, ACS Catal. **8**, 2995 (2018)
48. N.M.R. Martins, A.J.L. Pombeiro, L.M.D.R.S. Martins, Catal. Commun. **116**, 10 (2018)
49. G. Dixit, J.P. Singh, C.L. Chen, C.L. Dong, R.C. Srivastava, H.M. Agrawal, W.F. Pong, K. Asokan, J. Alloys Compd. **581**, 178 (2013)
50. K.N. Harish, H.S.B. Naik, P.N.P. Kumar, R. Viswanath, ACS Sustain. Chem. Eng. **1**, 1143 (2013)
51. S. Sagadevana, Z.Z. Chowdhuryb, R.F. Rafque, Mater. Res. **21**, e20160533 (2018)
52. R. Nivetha, C. Santhosh, P. Kollu, S.K. Jeong, A. Bhatnagar, A.N. Grace, J. Magn. Magn. Mater. **448**, 165 (2018)
53. M.M. Khalaf, H.M. Abd El-Lateef, G. Farghal, E.M.M. Ibrahim, Measurement **132**, 99 (2019)
54. E.M.M. Ibrahim, G. Farghal, M.M. Khalaf, H.M. Abd El-Lateef, Appl. Phys. A **123**, 533 (2017)
55. T.J. Shinde, A.B. Gadkari, P.N. Vasambekar, J. Alloys Compd. **513**, 80 (2012)
56. L. Chauhana, N. Singh, A. Dharb, H. Kumar, S. Kumar, K. Sreenivas, Ceram. Int. **43**, 8378 (2017)
57. M.S.S. Adam, A.M. Hafez, I. El-Ghamry, React. Kinet. Mech. Cat. **124**, 779 (2018)
58. M.S.S. Adam, M.S.M. Ahmed, O.M. El-Hady, S. Shaaban, Appl. Organometal. Chem. **34**, e5573 (2020)
59. J.J. Plata, L.C. Pacheco, E.R. Remesal, M.O. Masa, L. Vega, A.M. Márquez, J.A. Odriozola, J.F. Sanz, Mol. Catal. **459**, 55 (2018)
60. B.J. Hofmann, S. Huber, R.M. Reich, M. Drees, F.E. Kühn, J. Organomet. Chem. **885**, 32 (2019)
61. J. Du, C. Miao, C. Xia, Y.-M. Lee, W. Nam, W. Sun, ACS Catal. **8**, 4528 (2018)
62. S.M. Hosseini, H. Hosseini-Monfared, V. Abbasi, M.R. Khoshroo, Inorg. Chem. Commun. **67**, 72 (2016)
63. X. Liu, C. Manzur, N. Novoa, S. Celedón, D. Carrillo, J.-R. Hamon, Coord. Chem. Rev. **357**, 144 (2018)
64. M. Maurya, C. Haldar, A. Kumar, M.L. Kuznetsov, F. Avecilla, J.C. Pessoa, Dalton Trans. **42**, 11941 (2013)
65. G. Licini, V. Conte, A. Coletti, M. Mba, C. Zonta, Coord. Chem. Rev. **255**, 2345 (2011)
66. L. Gomez, I. Garcia-Bosch, A. Company, J. Benet-Buchholz, A. Polo, X. Sala, X. Ribas, M. Costas, Angew. Chem. Int. Ed. **48**, 5720 (2009)
67. M.R.M. Bisht, A. Kumar, M.L. Kuznetsov, F. Avecilla, J.C. Pessoa, Dalton Trans. **40**, 6968 (2011)
68. M.S.S. Adam, K.A. Soliman, H.M. Abd El-Lateef, Inorg. Chim. Acta **499**, 119212 (2020)
69. W. Yan, G. Zhang, H. Yan, Y. Liu, X. Chen, X. Feng, X. Jin, C. Yang, ACS Sustain. Chem. Eng. **6**, 4423 (2018)
70. D.-H. Zhang, G.-D. Li, J.-X. Li, J.-S. Chen, Chem. Commun. **29**, 3414 (2008)
71. Y. Zhang, Z. Li, W. Sun, C. Xia, Catal. Commun. **10**, 237 (2008)
72. G. Mata, R. Trujillano, M.A. Vicente, S.A. Korili, A. Gil, C. Belver, K.J. Ciuffi, E.J. Nassar, G.P. Ricci, A. Cestari, S. Nakagaki, Micropor. Mesopor. Mat. **124**, 218 (2009)
73. H. Mirzazadeh, M. Lashanizadegan, Solid State Sci. **79**, 48 (2018)
74. F. Shi, M.K. Tse, M.-M. Pohl, A. Bruckner, S. Zhang, M. Beller, Angew. Chem. Int. Ed. **46**, 8866 (2007)
75. S. Rayati, F. Ashouri, C. R. Chim. **15**, 679 (2012)
76. S. Huber, M. Cokoja, F.E. Kühn, J. Organomet. Chem. **751**, 25 (2014)
77. M. Nasrollahzadeh, M. Sajjadi, H.A. Khonakdar, J. Mol. Struct. **1161**, 453 (2018)
78. D.G. Reithwisch, J.A. Dumesic, Appl. Catal. **21**, 97 (1986)
79. A.M. Dumitrescu, P.M. Samoila, V. Nica, F. Doroei, A.R. Iordan, M.N. Palamaru, Powder Technol. **243**, 9 (2013)
80. K. Omata, T. Takado, S. Kasahara, M. Yamada, Appl. Catal. A **146**, 255 (1996)